Published in final edited form as:
Nat Chem Biol. 2019 February ; 15(2): 169–178. doi:10.1038/s41589-018-0195-0.

A Chemical Genetic Screen Identifies ABHD12 as an Oxidized Phosphatidylserine Lipase

Dhanashree S. Kelkar[#1], **Govindan Ravikumar**[#2], **Neelay Mehendale**[#1], **Shubham Singh**[#1], **Alaumy Joshi**[1], **Ajay Kumar Sharma**[2], **Amol Mhetre**[1], **Abinaya Rajendran**[1], **Harinath Chakrapani**[2], and **Siddhesh S. Kamat**[1,*]

[1]Department of Biology, Indian Institute of Science Education and Research (IISER), Dr. Homi Bhabha Road, Pashan, Pune

[2]Department of Chemistry, Indian Institute of Science Education and Research (IISER), Dr. Homi Bhabha Road, Pashan, Pune

[#] These authors contributed equally to this work.

Abstract

Reactive oxygen species (ROS) are transient, highly reactive intermediates or byproducts produced during oxygen metabolism. However, when innate mechanisms are unable to cope with sequestration of surplus ROS, it causes oxidative stress, where excess ROS damage biomolecules. Oxidized phosphatidylserine (PS), a pro-apoptotic “eat me” signal, is produced in response to elevated ROS, yet, little is known of its chemical composition and metabolism. Here, we report a small molecule that generates ROS in different mammalian cells, using which we detect, characterize and study oxidized PS in mammalian cells. We describe a chemical genetic screen to identify enzymes that regulate oxidized PS in mammalian cells, and find that the lipase ABHD12 hydrolyzes oxidized PS. We validate these findings in different physiological settings including primary peritoneal macrophages, and brains from *Abhd12*$^{-/-}$ knockout mice under inflammatory stress, and in the process functionally annotate an enzyme capable of regulating oxidized PS *in vivo*.

Oxidative stress is an imbalance between cellular oxidants and antioxidants in favor of oxidants, leading to disruption of redox signaling, and is implicated in several human pathophysiologies1–4. Under oxidative stress, excess ROS, namely superoxide, hydrogen

[*]To whom the correspondence should be made: siddhesh@iiserpune.ac.in.

Author Contributions

D.S.K., N.M., S.S., A.J., A.R. and S.S.K. performed the biochemical experiments and analyzed the data. G.R., A.K.S., A.M. and H.C. synthesized and chemically characterized all the chemical compounds in this study. D.S.K. and S.S.K. performed and analyzed the proteomics data. S.S.K. and H.C. conceived the project, and designed the experiments. S.S.K. wrote the paper with inputs from all authors.

Competing Financial Interests

The authors declare no competing financial interest.

Data Availability Statement

The authors declare that all the data that supports the findings of this study are available in the paper, and associated the supplementary information files and datasets.

peroxide (H_2O_2) and hydroxyl radicals, cannot be detoxified by innate mechanisms responsible to cope with them5, and these damage cellular components causing cell death via apoptosis or necrosis5. Lipid membranes are the cells first line of defense against ROS by providing a physical barrier to their diffusion, and therefore constitute primary targets for oxidative damage5. When ROS is generated near cellular membranes, the constituent lipids, in particular those bearing polyunsaturated fatty acid (PUFA) chains are oxidized6,7. The resulting oxidized lipids disrupt the local membrane structure and integrity, and thus impair cellular functions by modulating the activity of a wide array of important cellular proteins8,9. Previously, research groups have focused on the oxidation of a single PUFA6,7, and little is known of the global lipid profile under oxidative stress8,9, and the enzymatic pathways that metabolize these oxidized lipid products *in vivo*.

Phosphatidylserine (PS), an inner membrane leaflet localized phospholipid has several critical functions in mammalian biology10. Important amongst these, is its role in ROS signaling and apoptosis11. Given its asymmetry in the membrane bilayer, the externalization of PS reflects a stressed cell and this “flipped” PS is recognized by phagocytes as an “eat me” signal12–14. Several studies suggest that under oxidative stress, surplus ROS reacts with the *sn*-2 esterified PUFAs of PS, to produce oxidized PS6, which flips its membrane orientation, and acts as an apoptotic signal12,14. While these studies describe the production, and role of oxidized PS in apoptosis, little is known of its metabolism. Physiologically, this metabolism is important, as several cells require high oxygen tension (e.g. neurons, macrophages, cancers), and consequently have elevated ROS, that produce oxidized PS at a constant flux. Yet there exist innate mechanisms within such cells, which can efficiently metabolize oxidized PS, and prevent apoptosis.

In this paper, we describe a small molecule that generates ROS efficiently in mammalian cells, develop mass spectrometry methods to study oxidized PS, and using these in tandem, perform a chemical genetic screen to identify lipase(s) capable of metabolizing oxidized PS. We find that the serine hydrolase (SH) enzyme ABHD12 (α/β hydrolase domain (ABHD) protein # 12) is a major oxidized PS lipase. We validate these findings using complementary biochemical, pharmacological and genetic assays in different physiological systems. Importantly, we show that ABHD12 controls levels of oxidized PS in the mammalian brain under severe inflammatory stress. Given the central role of ABHD12 in PHARC, the human neurological disease15,16, its role in metabolizing oxidized PS, adds another avenue in understanding the PHARC pathophysiology.

Results

Characterization of an esterase activated ROS probe

1,4-Dihydroquinones react with oxygen to generate superoxide that spontaneously dismutates to hydrogen peroxide17,18. Amongst these, the “juglones” have proved effective against several antibiotic resistant bacteria19. Yet, very few probes of this scaffold are used to study ROS signaling in mammalian cells. The lack of intramolecular hydrogen bonding makes these molecules poor ROS generators17,18, hence installing a metabolically cleavable linker, that upon activation restores this, provides opportunities to trigger ROS generation on demand in mammalian cells. Using this rationale, we synthesized MGR1 (**1**),

5-hydroxy-1,4,4a,9a-tetrahydro-1,4-ethanoanthracene-9,10-dione (JCHD)17, with an esterase-activated handle (Fig. 1a). We postulated that MGR1 would be activated by ubiquitous esterase(s)20 in mammalian cells, and produce ROS (Supplementary Fig. 1). We also synthesized a structural analog, MGR2 (**2**), with a naphthalene moiety, unable to produce ROS, to control any structural effects of MGR1 (Fig. 1a). To validate the ROS production abilities of MGR1 and MGR2, we first performed a chemiluminescence assay21, and found that MGR1, but not MGR2, robustly produced ROS only when acted upon by an esterase (Fig. 1b). Consistent with the proposed mechanism (Supplementary Fig. 1), we found that pretreatment or incubation with a broad spectrum SH inhibitor (Fluorophosphonate-alkyne, FP-alkyne)20 or superoxide dismutase (SOD) respectively, ablated the ROS generating ability of MGR1 *in vitro* (Supplementary Fig. 2). Next, we detected 2-hydroxyethidium (2-HE) from hydroethidine due to superoxide from MGR1 only in the presence of esterase, by high performance liquid chromatography (HPLC) (Fig. 1c)22. SOD prevented 2-HE formation from MGR1 in the presence of an esterase, consistent with superoxide formation from MGR1 upon esterase activation (Fig. 1c). We also confirmed by HPLC analysis, that upon esterase activity, MGR1 and MGR2 produced JCHD, and 1-naphthol respectively (Supplementary Fig. 3).

Next we compared the ROS producing capability of MGR1 to MGR2, xenobiotics (menadione, artemisinin, cisplatin, paraquat), and ROS generators (JCHD, oxidized JCHD, H_2O_2) using the luminol based chemiluminescent assay (Supplementary Fig. 2), and the commercial 2',7'-dichlorodihydro-fluorescein diacetate (DCF) cellular ROS detection assay (Supplementary Fig. 4). We found from the chemiluminescent assay, that esterase treated MGR1 had comparable *in vitro* superoxide production to JCHD, and these were significantly higher than any ROS generator and/or xenobiotic tested at a comparable concentration (Supplementary Fig. 2). We then treated HEK293T cells with MGR1, or MGR2, or xenobiotics, or ROS generators (25 μM, 1 h (H_2O_2 = 1 mM), followed by 10 μM DCF, 10 min), and imaged the cellular fluorescence due to ROS. We found that MGR1, but not MGR2, robustly produced ROS in HEK293T cells, and MGR1 was the best ROS generator compared to other xenobiotics and/or ROS generators (Fig. 1d, Supplementary Fig. 5). Additionally our prodrug approach of using MGR1 instead of JCHD results in more ROS production at the same MGR1 and JCHD concentrations, due to better MGR1 bioavailability (Supplementary Fig. 5). Similar results were found from other mammalian cell lines (Supplementary Fig. 5). To determine if the surplus ROS from MGR1 affected the cellular viability, the dose dependence of MGR1 and MGR2 in different mammalian cell lines was assessed. In HEK293T cells, we found concentration dependent cell death following MGR1 (IC_{50} ~ 5.7 ± 0.6 μM), but not MGR2 (IC_{50} > 40 μM) treatment (Fig. 1e). Similar results were seen in other mammalian cell lines (Supplementary Fig. 6). To confirm the cell death was ROS dependent, we pretreated mammalian cells with antioxidants, Pterostilbene (PTS, 10 μM)23 or *N*-acetyl-cysteine (NAC, 1 mM)24, following which, the cells were treated with MGR1, and ROS production was assessed. We found both PTS and NAC substantially reduced the cellular ROS after MGR1 treatment (Supplementary Fig. 7). Additionally, the cell death caused by MGR1 treatment in different mammalian cell lines was also rescued by PTS or NAC, further confirming that reduced cellular viability was due to surplus ROS from MGR1 (Supplementary Fig. 8). For subsequent cellular studies, we

required a concentration of MGR1 that produces elevated ROS, not enough to cause cell death, and chose 2 μM MGR1 or MGR2 (4 h) as the treatment paradigm (Fig. 1e, Supplementary Fig. 6).

A quinone (JCHD) is produced from MGR1, and quinones are known to form covalent adducts with protein thiols25,26. To determine the thiol reactivity of MGR1 relative to reactive quinones, we performed a gel-based chemoproteomics using iodoacetamide-alkyne (IAA) as an activity reporter of cellular thiols27. In this experiment, HEK293T and RAW264.7 cell lysates were treated with the reactive quinones or MGR1 (+ esterase) (all 100 μM, 1 h), chased with IAA (1 mM, 1 h), following which click reaction was performed28, and the proteome was resolved and visualized by SDS-PAGE gel. We found negligible proteome wide thiol reactivity for MGR1 (or JCHD) relative to reactive quinones (Fig. 1f). Mass spectrometry based chemoproteomics further confirmed negligible proteome wide thiol and serine reactivity of MGR1 (2 μM, 4 h) in HEK293T cells (Supplementary Fig. 9–12, Supplementary Dataset 1), suggesting the cell death was caused by MGR1 was due to surplus ROS, and not thiol modification by the quinone product.

Measurements of oxidized PS in cells

Our interest in understanding the oxidized PS metabolism under oxidative stress stems from its importance in programmed cell death12, and we decided to establish a LC-MS/MS method to measure these. We first treated C18:0/18:1PS (1-stearoyl-2-oleoyl-*sn*-glycero-3-phospho-L-serine, 100 μg) with excess H_2O_2 (10 mM) in the presence of iron (II) (1 mM), and ascorbate (1 mM) to produce ROS by Fenton and Haber-Weiss chemistry29. We found in addition to the native mass of 788.5445 ([M-H]: C18:0/18:1PS), two new masses 804.5392, and 806.5549 were observed (Fig. 2a). We performed MS/MS on these masses, and found that 804.5392 and 806.5549 are +16 (O), and +18 (H_2O) additions respectively. The MS/MS fragmentations for both these masses, suggested that mass additions of +16 (m/z = 297.2431) and +18 (m/z = 299.2590), were present on the *sn-2* oleate of C18:0/18:1PS, forming an epoxide and hydroxide respectively (Fig. 2a, Supplementary Fig. 13, Supplementary Note). We termed the +16 and +18 mass additions as ox- and hy- respectively. We hypothesized that the oxygenation of C18:0/18:1PS, would increase its hydrophilicity, and the resulting oxygenated species would elute at lesser time on a C18 column. Indeed, this is what we observed, where ox-18:0/18:1PS, and hy-18:0/18:1PS eluted at 27.8 and 27.1 min respectively, while C18:0/18:1PS eluted at 32.3 min in our LC-MS/MS method30 (Fig. 2b). C18:1 lyso-PS eluted at 24.9 min, suggesting that both ox-18:0/18:1PS, and hy-18:0/18:1PS, were more lipophilic than C18:1 lyso-PS, because of an additional fatty acid (Fig. 2b). Corroborating the LC-MS/MS findings, thin layer chromatography (TLC)31 showed a distinct spot for oxidized PS between PS and lyso-PS (Supplementary Fig. 14).

To determine, if MGR1 produces oxidized PS, we treated HEK293T cells with MGR1 or MGR2 or DMSO (2 μM, 4 h), and extracted the phospholipids30,32. We detected m/z = 788.5445, in all treatment groups, but m/z = 804.5392, and 806.5549, were found enriched following MGR1 treatment. To determine, if these masses correspond to C18:0/18:1PS, and the synthetic ox-18:0/18:1PS, and hy-18:0/18:1PS, we performed MS/MS analysis on endogenous m/z = 788.5445, 804.5392, and 806.5549, from phospholipids extracted from

MGR1 treated cells, and found that the MS/MS fragmentations for the endogenous masses exactly matched the synthetic standards. Notably, all three masses showed peaks at the parent m/z minus 87.0315 (loss of serine), 437.2671 (1-stearoyl-2-hydroxy-*sn*-glycero-3-phosphate), 419.2562 (dehydro-1-stearoyl-2-hydroxy-*sn*-glycero-3-phosphate), 283.2640 (stearate), and 152.9951 (dehydro-glycerophosphate) (Fig. 2a). We also detected m/z = 297.2433 and 299.2590 in the MS/MS fragmentations of endogenous 804.5392, and 806.5549 respectively, confirming the formation of +16 (epoxy) and +18 (hydroxide) oxygenated adducts described earlier for ox-18:0/18:1PS, and hy-18:0/18:1PS respectively (Fig. 2a).

The MS/MS fragmentation helped us develop a targeted multiple reaction monitoring (MRM) LC-MS/MS method to quantitate different oxidized PS species (Supplementary Dataset 2). We validated this, by quantifying ox-18:0/18:1PS, and hy-18:0/18:1PS from HEK293T cells treated with MGR1 or MGR2 or DMSO (2 μM, 4 h), and found that MGR1 treated cells have substantially more ox-18:0/18:1PS and hy-18:0/18:1PS compared to MGR2 or DMSO treated cells, with similar elution times to the synthetic standards (Fig. 2c, Supplementary Fig. 13). Next, we measured different ox- and hy-PS after MGR1 and MGR2 treatments in HEK293T cells, and found that several ox-PS and hy-PS were significantly elevated upon MGR1, but not MGR2 or DMSO treatment (Fig. 2d). Notably, all detected oxidized PS bear an unsaturated fatty acid esterified at the *sn-2* position, where the oxygenation likely occurs. We found no change in cellular PS or lyso-PS, and were unable to detect oxidized PS secreted from HEK293T cells following MGR1 or MGR2 treatment (Supplementary Dataset 2). Similar results were observed in other mammalian cell lines (Supplementary Fig. 15, Supplementary Dataset 2).

Chemical genetic screen to identify oxidized PS lipase(s)

To better understand oxidized PS metabolism, we developed a screen to identify enzyme(s) that hydrolyzes oxidized PS lipids using the aforementioned LC-MS/MS method. At the onset, we hypothesized that a lipase (likely a metabolic SH) would perform this activity20,33. Hence we needed a cell line that expressed many SHs and had high lipid content for our screen. Public databases34 have shown that RAW264.7 macrophages fulfill these criteria, and was chosen as the candidate cell line for the screen. We collated a focused library of 57 compounds, ranging from specific to broad-spectrum lipase inhibitors (Supplementary Dataset 3)20,33. We treated RAW264.7 cells with inhibitor (10 μM, 4 h), followed by treatment with MGR1 (5 μM, 4 h), after which we extracted cellular phospholipids, and analyzed the oxidized PS by targeted LC-MS/MS (Supplementary Fig. 16). As screening controls, MGR2 and DMSO were used. We set 2-fold accumulation in cellular oxidized PS as a threshold for identifying hits from the screen, and found that most inhibitors had no effect on oxidized PS (comparable to DMSO post MGR1 treatment). Three compounds however, FP-alkyne, tetrahydrolipstatin (THL, also orlistat) and methylarachidonyl fluorophosphonate (MAFP), showed > 2-fold increase in cellular oxidized PS (Fig. 3a). Both FP-alkyne and MAFP are broad-spectrum SH inhibitors20, further confirming that the lipase(s) of interest was a SH. Since FP-alkyne and MAFP have several enzyme targets, we focused on THL, as this β-lactone inhibitor potently inhibits only a handful of SHs35.

To determine targets of THL in RAW264.7 cells, we employed competitive activity based protein profiling (ABPP) assays. We treated RAW264.7 cells with THL (10 μM, 4 h), and assessed the membrane and soluble proteomes by competitive gel-based ABPP (Fig. 3b, Supplementary Fig. 17)32. Following THL treatment, we found no activity loss in the soluble proteome, while the membrane proteome showed few enzymes whose activity was inhibited. Prominent amongst these was a SH ~42 kDa, likely ABHD12, a known THL target (Fig. 3b, Supplementary Fig. 17)35. Next, we coupled ABPP (using a biotinylated FP-probe, FP-biotin)36 to LC-MS/MS analysis32, and identified 34 SHs, of which 12 were inhibited > 90% (THL, 10 μM, 4 h). Not surprisingly, there were 7 lipases: (i) ABHD6, (ii) neuropathy target esterase (PNPLA6), (iii) hormone sensitive lipase (HSL or LIPE), (iv) ABHD16A, (v) patatin-like phospholipase domain containing protein 7 (PNPLA7), (vi) cytosolic phospholipase A2 (PLA2G4A), and (vii) ABHD12, amongst these targets (Fig. 3c, Supplementary Dataset 4). Besides these, diacylglycerol lipase beta (DAGLβ) and lipoprotein-associated phospholipase A2 (PLA2G7) are also targets of THL35. We detected DAGLβ, but surprisingly, were unable to see significant inhibition of DAGLβ (Supplementary Dataset 4). We did not detect PLA2G7 in our experiments. Our chemical genetic screen contained specific inhibitors for most THL targets, and these showed almost no effect on cellular oxidized PS in the screen (KT195, WWL70: ABHD6; Palmostatin-B: PNPLA6; BAY, Cay10499: HSL; KC01: ABHD16A; Pyrrophenone: PLA2G4A; KT109, KT172: DAGLβ; Darapladib, JMN4: PLA2G7) (Supplementary Dataset 3). This enabled elimination of most lipase targets of THL, except ABHD12 and PNPLA7, suggesting that one of these lipases was likely an oxidized PS lipase. Nonetheless, we overexpressed all the lipase targets of THL in HEK293T cells, and tested these lysates for substrate hydrolysis activity against lyso-PS, oxidized PS and PS. Additionally, we tested the SHs ABHD337 and PNPLA838 as well, since these have been reported to hydrolyze oxidized phospholipids. We found amongst all candidate lipases that ABHD12 was the best candidate, with > 3-fold hydrolysis rate for oxidized PS than any other lipase (Supplementary Fig. 18). As expected, ABHD12 had robust activity against lyso-PS, but not PS (Supplementary Fig. 18)39, suggesting that this enzyme can use both lyso-PS and oxidized PS as substrates *in vitro*.

Biological validation of ABHD12 as an oxidized PS lipase

To validate if ABHD12 was indeed an oxidized PS lipase, we first generated the catalytically “dead” S246A mutant of human ABHD12 (hABHD12), and overexpressed S246A hABHD12 or wild type (WT) hABHD12 or an empty plasmid (mock) in HEK293T cells. Western blot analysis confirmed WT hABHD12 and S246A hABHD12 were overexpressed in HEK293T membranes, and gel-based ABPP confirmed S246A hABHD12 was inactive (Fig. 4a). We also confirmed that WT hABHD12 was potently inhibited by THL (Supplementary Fig. 19)35. First, we tested mock or WT hABHD12 or S246A hABHD12 overexpressing HEK293T membrane lysates against lyso-PS, oxidized PS or PS32,39, and found that WT hABHD12 efficiently hydrolyzes lyso-PS and oxidized PS, at comparable rates, with no activity against PS (Fig. 4b). S246A hABHD12 and mock HEK293T membrane lysates had negligible activity against all three substrates (Fig. 4b). Next, we tested if heightened ABHD12 activity had any effect on cell viability following MGR1 treatment. Here, HEK293T cells transfected with mock, or WT hABHD12 or S246A hABHD12, were treated with MGR1 (0 – 40 μM, 4 h), and the viable cells were quantified.

We found that mock (IC_{50} = 1.7 ± 0.6 μM) and S246A hABHD12 (IC_{50} = 1.9 ± 0.4 μM) had comparable cell viability profiles following MGR1 treatment, while the increased activity of WT hABHD12 partly protected against MGR1 treatment (IC_{50} = 13.9 ± 2.4 μM) (Fig. 4c).

Further, we tested if overexpressing WT hABHD12 had any effect of cellular oxidized PS. Here, HEK293T transfected with mock or WT hABHD12 or S246A hABHD12, were treated with MGR1 (2 μM, 4 h), following which cellular oxidized PS was quantified. We found cells overexpressing WT hABHD12 had significantly lower cellular oxidized PS compared to mock or S246A hABHD12 overexpressing cells (Fig. 4d, Supplementary Dataset 2), consistent with WT hABHD12's, but not S246A hABHD12's, ability to hydrolyze oxidized PS. Finally, we tested if the pharmacological blockade of ABHD12 had any effect on cellular oxidized PS. In the absence of any reported ABHD12 selective cell active inhibitor, we treated RAW264.7 cells with increasing THL (0 – 10 μM, 4 h), and found a dose dependent increase in oxidized PS following THL treatment (Fig. 4e, Supplementary Dataset 2). This result suggests that acute blockade of ABHD12 activity controls cellular oxidized PS.

ABHD12 functions as an oxidized PS lipase *in vivo*

To physiologically complement our studies, we first investigated oxidized PS from primary peritoneal macrophages (PPM) harvested from WT or ABHD12 knockout mice. We found that lipopolysaccharide (LPS) stimulation of PPM increases the cellular ROS and lyso-PS, and ABHD12 controls secreted lyso-PS32,40 (Supplementary Fig. 20, 21, Supplementary Dataset 2). Interestingly, PPM from WT mice, showed 2-fold increase in the cellular oxidized PS upon LPS stimulation, corroborating the increased cellular ROS in PPM following LPS stimulation40 (Fig. 5a, Supplementary Dataset 2). Remarkably, we found in both vehicle and LPS treatments, PPM from ABHD12 knockout mice always have ~2-fold more cellular oxidized PS than PPM from WT mice (Fig. 5a, Supplementary Dataset 2). We could not detect any oxidized PS secretion from PPM from either genotype. Next, we tested if oxidized PS identified by us has any role in immune activation. To assess this, we incubated PPM from WT or ABHD12 knockout mice, with freshly prepared oxidized PS (mixture of ox-18:0/18:1PS and hy-18:0/18:1PS), or C18:0/18:1PS or C18:1 lyso-PS or LPS (all 10 μg/mL, 4 h), and measured proinflammatory cytokines secretion from these cells. We found from WT PPM, that oxidized PS produces 10- and 5-fold more secretion of TNF-α and IL-6 compared to the vehicle (or C18:0/18:1PS) and lyso-PS control groups respectively, and about half of that from the LPS treatment group (Fig. 5b). When comparing the WT and ABHD12 knockout groups, we find that across all treatments, PPM from ABHD12 knockout mice always secrete more TNF-α and IL-6. Notably, oxidized PS treatment of PPM from ABHD12 knockout mice, shows the highest response, with ~2-fold increase in TNF-α and IL-6 secretions, compared to WT PPM (Fig. 5b). Similar increased proinflammatory cytokine secretion following oxidized PS treatment was seen in THP1 macrophages (Supplementary Fig. 22), suggesting that oxidized PS is a more potent immunostimulatory lipid than lyso-PS or PS.

Finally, we looked for oxidized PS in the brains of WT and ABHD12 knockout mice, but were unable to detect these in either genotype for the mice *ab libitum*. So, we induced

neuroinflammation in these mice by intraperitoneal LPS injections using two paradigms41: (i) high dose acute (20 mg/kg, 6 h) and (ii) low dose chronic (1 mg/kg, q. d., 4 d); to check if oxidized PS is produced as these neuroinflammatory LPS stimuli are known to generate enhanced ROS in the mammalian brain42,43. We confirmed that the neuroinflammatory challenges were effective by measuring increased prostaglandin and proinflammatory cytokines in the brains of the LPS treated mice (Supplementary Fig. 23). Interestingly, we found that mice from the low dose chronic treatment showed negligible accumulation of oxidized PS, but mice from high dose acute treatment showed significant accumulation of oxidized PS in the brain (Fig. 5c, Supplementary Dataset 2). The oxidized PS accumulation between these genotypes was most pronounced for the high dose acute treatment, with the ABHD12 knockout brains showing > 5-fold accumulation of oxidized PS relative to similarly treated WT mice (Fig. 5c). We found that ABHD12 knockout mice brains always had higher brain lyso-PS content compared to similarly treated WT mice, but the lyso-PS levels did not change during the LPS treatments (Supplementary Fig. 24, Supplementary Dataset 2). Quite interestingly, we find that proinflammatory cytokines are also significantly elevated in the brains of ABHD12 knockout brains from the high dose acute LPS treatments (Supplementary Fig. 23).

Discussion

The oxidation of PS due to elevated ROS is linked to its transmembrane migration, and presence on the exofacial membrane surface (Supplementary Fig. 25)14,44, where oxidized PS externalization generates an “eat me” signal, making it recognizable to a phagocyte12. An elegant study showed apoptotic cells are indeed cleared by macrophages, through specific recognition of externalized oxidized PS by a B-type scavenger receptor13. Additionally, the cellular protein, annexin-V, is known to bind externalized oxidized PS, and several kits for this protein-lipid interaction are used to quantitatively measure apoptotic cells. While PS oxidation, and its role in apoptosis are well understood, little is known of the enzymatic pathways that metabolize oxidized PS *in vivo*.

In this study, we wanted to identify an enzyme capable of metabolizing oxidized PS in mammalian cells. Towards achieving this, we synthesized a chemical probe robustly generating ROS in mammalian cells, enabling us to mimic oxidative stress (Fig. 1). Next, we developed a LC-MS/MS method to identify and quantitate oxidized PS in mammalian cells, and found two new oxidized PS species, which we termed ox-PS and hy-PS, to exist in different mammalian cells in response to oxidative stress (Fig. 2). We performed a chemical genetic screen to identify an enzyme capable of metabolizing oxidized PS in mammalian cells, and identified ABHD12 as a likely candidate (Fig. 3). We provide compelling biochemical, pharmacological and genetic evidence in support of ABHD12 being a major lipase capable of hydrolyzing oxidized PS (Fig. 4, 5).

ABHD12 has tremendous biomedical interest, as it is linked to the human neurodegenerative disease PHARC, caused by null mutations to *abhd12*15,16. ABHD12 is annotated as a lyso-PS lipase in the mammalian brain and immune system16,32,39,45. Lipidomics on PPM from ABHD12 knockout mice39 and human PHARC subject lymphoblasts16 show that ABHD12 controls levels of secreted lyso-PS, but not cellular lyso-PS32. This is not

surprising, as the active site of ABHD12 is extracellularly orientated32,45,46. It is this active site orientation, which we believe, allows it access to exofacially oriented oxidized PS generated by elevated cellular ROS during oxidative stress (Supplementary Fig. 25). Our studies, thus posit a dual role for ABHD12, where it regulates the cellular oxidized PS and the secreted lyso-PS, independently or simultaneously (e.g. PPM). We also show that the newly identified oxidized PS elicit immune responses in PPM through heightened secretion of proinflammatory cytokines, with more pronounced responses in ABHD12-null PPM. Finally, we show that ABHD12 controls oxidized PS levels in the mammalian brain and in turn proinflammatory cytokines under severe neuroinflammatory stimuli. Taken together, our studies build on the existing model that describes the progression of the PHARC pathology. We propose, like other neurodegenerative disorders, oxidative stress and ROS may also play a role in the PHARC pathology, and simplistically ABHD12 mitigates excess oxidized PS produced in this process (Fig. 5d).

Projecting forward, gene expression studies34 suggest that ABHD12 is expressed mostly in the nervous and immune system, yet PS is known to exist in metabolic tissues susceptible to oxidative stress11. Hence there must exist resident lipases besides ABHD12 that metabolize oxidized PS in these tissues. We believe the tools and methods described here might offer an elegant strategy in functionally annotating such lipases. In addition, developing new tools that allow visualization of oxidized PS *in vivo* would be beneficial in understanding the spatiotemporal distribution and regulation of these lipids in diverse biological settings. Also, the protein ligands and/or receptors for oxidized PS are largely unknown. Thus finding, and understanding downstream biological signaling pathways using emerging chemoproteomics platforms47,48 would advance this lipid-signaling field, and shed new insights into programmed cell death. Finally, recent functional studies have shown that other metabolic SHs are regulators of other oxidized phospholipids *in vivo*49,50. We believe that the emerging functional annotation of orphan SHs might implicate their role in the regulation of oxidized lipids from other lipid classes (neutral lipids, sterols) and in doing some, increase the repertoire of oxidized lipids under oxidative stress.

Online Methods

Materials

All chemicals, buffers, and reagents were purchased from Sigma-Aldrich, all lipids and lipid standards were purchased from Avanti Polar Lipids Inc., and all primary and secondary antibodies were purchased from Abcam, unless otherwise mentioned. The mouse or human inflammatory cytokine single analyte ELISA kits were purchased from R&D Systems for cytokine measurements.

Mammalian cell culture and treatment

All mammalian cell lines were purchased from ATCC, and cultured in RPMI1640 medium (HiMedia) supplemented with 10% (v/v) Fetal Bovine Serum (FBS) (Invitrogen) and 1x penicillin-streptomycin (MP Biomedicals) at 37 °C with 5% (v/v) CO_2. All cell lines were routinely stained with DAPI to ensure they were devoid of any mycoplasma contamination. All cell viability studies for MGR1 and MGR2 treatments were done using a TC20

Automated Cell Counter with Trypan Blue reagent (Bio-Rad) as per manufacturers instructions. Briefly, cells were treated with varying concentrations (0 – 40 μM) of MGR1 or MGR2 for 4 h, at which point, the cells were detached by trypsinization and live cells were estimated as per manufacturers protocol. For lipid measurements, $2x10^6$ cells were washed with sterile Dulbecco's Phosphate Buffer Saline (DPBS) (HiMedia) (3X) and treated with MGR1 (2 μM) or MGR2 (2 μM) or DMSO for 4 h at 37 °C and 5% (v/v) CO_2 in 5 mL of aforementioned media (10 cm tissue culture dish). Post treatment, the cells were washed again with sterile DPBS (3X), and the lipids were extracted immediately using the protocol described below. All cellular ROS chemifluorescence imaging were performed using the DCF dye (10 μM, 10 min, Thermofisher Scientific) on an EVOS® FL Auto Imaging System (Life Technologies, Thermofisher Scientific) as per manufacturer's instructions.

Preparation of oxidized PS

Oxidized PS was generated using an established protocol with slight modifications29. Briefly, 100 μg of PS (C18:0/18:1PS) was resuspended in 900 μL DPBS by sonication, and incubated at 37 °C for 5 min, with shaking. To this PS suspension, 90 μL of H_2O_2 (11 mM) was added and incubated at 37 °C for 5 min with shaking. The PS oxidation was initiated by adding 10 μL mixture of ferrous ammonium sulfate (100 mM) and ascorbate (100 mM), and allowed to proceed at 37 °C for 30 min with shaking. The reaction was quenched as described29, and preparative HPLC procedure (see Supplementary Note) was used to purify the oxidized PS. The purity of oxidized PS was assessed first by thin layer chromatography (TLC)31 (Supplementary Fig. 14) and ^{1}H-NMR analysis, and the identity was further confirmed by lipid fragmentation analysis described in the next section, ^{1}H-NMR and IR spectroscopic analysis (see Supplementary Note). Based on the TLC, LC-MS/MS and ^{1}H-NMR analysis, our oxidized PS preparations are ~ 95% pure, with some contamination from the unreacted starting PS (see Supplementary Note).

Lipid fragmentation analysis

All lipid fragmentation studies were performed by LC-MS/MS analysis on a Sciex X500R Quadrupole Time Of Flight (QTOF) mass spectrometer fitted with an Exion series UHPLC with a quaternary pump. The LC separation was achieved on a Gemini 5U C18 column (Phenomenex, 5 μm, 50x4.6 mm) coupled to a Gemini guard column (Phenomenex, 4x3 mm, Phenomenex security cartridge). All PS, lyso-PS and oxidized PS lipids were analyzed in the negative ionization mode using: solvent A: 95:5 (v/v) H_2O: methanol (MeOH) + 0.1% ammonium hydroxide; and solvent B: 60:35:5 (v/v) isopropanol: MeOH: H_2O + 0.1% ammonium hydroxide using an established LC method on an electrospray ion (ESI) source30,39. The $[M–H]^-$ of the lipid standards and m/z values of the endogenous lipids were comparatively assessed by LC-MS/MS analysis. The lipid extraction protocol for the endogenous lipids is described briefly in the section below. The total scan time for both the MS1 and MS2 spectra was 2.5 s, and the collision energy (volts) of –30, –40 and –52 for lyso-PS, oxidized PS and PS were respectively used. The declustering potential and ion source voltage were set at –110 and –5500 volts respectively. The drying gas temperature was 550 °C, drying gas flow rate was 15 L/min, and the nebulizer (ion source gas) pressure was 50 psi for this lipid fragmentation study.

Quantitative lipid measurements

The phospholipid extractions were done using an established protocol based on the Folch lipid extraction method30,32,51. Briefly, the cells were washed with sterile DPBS (3X), and transferred into a glass vial using 1 mL sterile DPBS. 3 mL of 2:1 (v/v) chloroform ($CHCl_3$): MeOH with the lipid internal standard mix (internal standards listed in Supplementary Dataset 2) was added, and the mixture was vortexed. The two phases were separated by centrifugation (2800g, 5 min). The organic phase (bottom) was removed, 50 μL of formic acid was added to acidify the aqueous homogenate (to enhance phospholipid extraction), and $CHCl_3$ was added to make up 4 mL volume. The mixture was vortexed, and separated by centrifugation (2800g, 5 min). Both the organic extracts were pooled, and dried under a stream of N_2 gas. The dried organic phase containing the phospholipids of interest was resolubilized in 150 μL of 2:1 (v/v) $CHCl_3$: MeOH, and 20 μL was used for the targeted LC-MS/MS analysis. All the lipid species analyzed in this study were quantified using the multiple reaction monitoring high resolution (MRM-HR) method on a Sciex X500R QTOF fitted with an Exion series UHPLC with a quaternary pump. All data was collected and analyzed using SciexOS software. All lipid estimations were performed using an ESI source, with the following MS parameters: curtain gas = 20 L/min, ion spray voltage = –5500 V, temperature = 550 °C. The LC separation, buffers and method were the same as described earlier30,32. A scheduled MRM-HR program was used to measure lyso-PS lipids only between 22 – 28 mins, oxidized PS lipids only between 25 – 30 mins, and PS lipids only between 30 – 38 mins, to get better sensitivity for the quantitative lipid measurements. A detailed list of all the lipid species targeted in this MRM-HR study, describing the precursor parent ion mass, the product ion targeted, and other compound specific voltages and parameters, and the internal standard for the respective lipid class can be found in Supplementary Dataset 2. All endogenous PS and lyso-PS lipids were quantified by measuring the area under the curve relative to the respective internal standard, and then normalizing to the total cellular protein content or cell number as applicable. For oxidized PS lipid species, C12:0/13:0PS was used as an internal standard. All the data is represented as mean ± s.e.m. of 4 or more biological replicates per study group (Supplementary Dataset 2). It is important to note that all oxidized PS measurements were done with fresh preparations, as the endogenous oxidized PS lipids are susceptible to degradation post extraction from mechanisms not fully clear. The oxidized PS synthetic standards are stable for 1 week when stored at –40 °C.

Chemical genetic screen

RAW264.7 cells ($1x10^6$ cells) were cultured in 6 well plates in media described earlier. The cells were treated with lipase inhibitor (10 μM, 4 h), following which the cells were washed with sterile DPBS (3X), and replaced with the same fresh media. The cells were then treated with MGR1 (5 μM, 4 h), subsequently washed with sterile DPBS (3X), and lipids extracted to perform quantitative lipid measurements. As a control for the lipase inhibitor group, DMSO was used, while MGR2 (5 μM) and DMSO were used as controls for MGR1 treatments. Each treatment group at least three biological replicates.

Gel-based ABPP

Gel-based ABPP experiments were done using established protocols36,52. Briefly, cell pellets were resuspended in 1 mL cold sterile DPBS, lysed by sonication, and the lysates were centrifuged at 100,000g for 45 mins. The supernatant (soluble proteome) was collected, and the remaining pellet was washed with sterile DPBS (3X), and resuspended in cold sterile DPBS to yield the membrane proteome. Protein concentrations were estimated using the Pierce BCA Protein Assay kit (Thermofisher Scientific). Proteomes (1 mg/mL, 100 μL) were treated with FP-rhodamine (2 μM, 45 min, 37 °C) with constant shaking (750 rpm). Addition of 4X-SDS loading buffer followed by boiling the samples (95 °C, 10 min) quenched the reactions. Fluorescently labeled proteomes were resolved on a 10% SDS-PAGE gel and samples were visualized on a Syngene G-Box Chemi-XRQ gel documentation system. Competitive gel-based ABPP with THL was performed as described earlier32,35.

Western blot analysis

Soluble or membrane proteomes or cell lysates were separated on a 10% SDS-PAGE gel, and transferred onto a PVDF membrane (GE Healthcare) (60V, 12 h, 4 °C). Post-transfer, the membrane was blocked using 5% (w/v) milk in TBST, and subsequently probed with a primary antibody (dilution 1:1000). An anti-rabbit IgG (H+L) HRP conjugated (goat, Thermofisher Scientific, 31460, dilution 1:10,000) was used a secondary antibody, and the signal was visualized using the SuperSignal West Pico Plus Chemiluminescent substrate (Thermofisher Scientific) using a Syngene G-Box Chemi-XRQ gel documentation system. All primary antibodies used in this study have been mentioned along with source, and catalog number, wherever mentioned in the paper.

Identification of THL targets from RAW264.7 cells

$1x10^7$ RAW264.7 cells were treated with THL (10 μM, 4h) or DMSO (4 h) in media described earlier. Post-treatment, the cells were harvested by scrapping, and lysed by sonication, and whole cell lysates were used in this experiment. For proteomics sample preparations, cell lysates (2 mg/mL in 1 mL DPBS) were labeled with FP-biotin (10 μM, 1 h, 37 °C with shaking). Post-labeling, the proteomes were denatured and precipitated using 4:1 MeOH: $CHCl_3$ at 4 °C, resuspended in 0.5 mL of 6 M urea in DPBS by sonication, sequentially reduced by Tris(2-carboxyethyl)phosphine (TCEP, 10 mM, 30 min, 37 °C with shaking), and alkylated by iodoacetamide (50 mM, 30 min, 25 °C) in the dark. The biotinylated proteins were enriched with prewashed (DPBS-washed (3X)) avidin-agarose beads (100 μL, Sigma-Aldrich) by shaking 25 °C for 90 min in DPBS containing 2% (w/v) SDS in 6 mL final volume. The beads were pelleted by centrifugation at 1000g for 5 min, and washed as described earlier32. The beads were transferred to a Protein LoBind tube (Eppendorf, 1.5 mL) using 1 mL triethylammonium bicarbonate (TEAB, 100 mM) buffer, pelleted by centrifugation at 1000g for 5 min, and the buffer was aspirated. On bead protein digestion was performed using sequence grade trypsin (2 μg, Promega) in 100 mM TEAB buffer containing 2 M urea for 14 h at 37 °C with constant shaking in a final volume of 200 μL. The downstream reductive dimethylation labeling was performed as per protocols described earlier using light (H_2CO) and heavy (D_2CO) formaldehyde and sodium

cyanoborohydride ($NaBH_3CN$)32,53. Peptides from THL treated group (light labeled) and DMSO treated group (heavy labeled) were mixed and cleaned using StageTip protocol54. All LC-MS/MS analysis was performed on a Sciex TripleTOF6600 mass spectrometer interfaced with an Eksigent nano-LC 425. 1 μg tryptic peptides were loaded onto an Eksigent C18 trap (5 μg capacity), and subsequently eluted on an Eksigent C18 analytical column (15 cm x 75 μm internal diameter) with a linear acetonitrile gradient. A typical LC run consisted of 2 h post loading onto the trap at a constant flow rate of 300 nL/min with solvents A = water + 0.1% formic acid, and B = acetonitrile. The gradient schedule for the LC run was: 5% (v/v) B for 10 min, a linear gradient of B from 0 – 80% (v/v) over 80 min, 80% (v/v) B for 15 min, and equilibration with 5% (v/v) B for 15 min. For all proteomics samples, data was acquired in information dependent acquisition (IDA) mode over a mass range of 300 – 2000 m/z. Each full MS survey scan was followed by MS/MS of the 15 most intense peptides. Dynamic exclusion was enabled for all experiments (repeat count 1, exclusion duration 6s). Peptide identification and quantification was carried out using MaxQuant1.755. A Refseq mouse protein database (release 86) including contaminant protein sequences was used for peptide identification. The peptide searches in MaxQuant1.7 algorithm specified +57.0215 m/z iodoacetamide alkylation of cysteine as a static modification, while methionine oxidation and N-terminal acetylation were specified as variable modifications. A precursor ion and MS/MS mass tolerance was set at 20 and 40 ppm respectively for the peptide searches. For reductive dimethylation based quantification of tryptic peptides, the N-terminal and lysine dimethyl labels were specified as fixed modifications in search algorithm. The PSM level false positive discovery rate (FDR) was calculated using decoy database search, and the peptides and proteins were filtered for < 1% FDR. Serine hydrolase enzymes identified in all replicates, and having ≥ 2 quantified peptides were filtered for this study.

Expression of recombinant human ABHD12

The full-length hABHD12 cDNA was cloned into pCMV-Sport6 vector between NotI and SalI restriction sites (GE Life Sciences). The S246A hABHD12 mutant was generated from the same plasmid using Phusion polymerase and DpnI (New England Biolabs) as per manufacturers instructions. Recombinant WT and S246A hABHD12 was generated from HEK293T cells using established transient transfection protocols32. “Mock” control cells were transfected with an empty vector using the same protocol. The cells were harvested by scraping 48 h after transfection, washed with sterile DPBS (3X), resuspended in 1 mL DPBS, and lysed by sonication. The overexpression of hABHD12 was confirmed by gel-based ABPP and western blot analysis on membrane proteomes of the transfected cells, preparations of which are described earlier.

Substrate assays

The membrane proteome of HEK293T transfected cells (20 μg) was incubated with 100 μM lipid substrate in DPBS (100 μL total volume) at 37 °C with constant shaking (750 rpm). After 30 min, the reaction was quenched by addition of 350 μL of 2:1 $CHCl_3$: MeOH containing 1 nmol of each internal standard (heptadecenoic acid and C17:1 lyso-PS). The subsequent lipid enrichments, separation and LC-MS analysis were done using a previously established protocol32,39. Measuring the area under the curve and normalizing to the

respective internal standard was used to quantify the product release. The non-enzymatic rate of substrate hydrolysis was obtained by using heat-denatured proteomes, and this value was subtracted from the substrate hydrolysis rates of native proteomes to yield the corrected rates. For lyso-PS substrates, only the release of free fatty acid was quantified, while for PS and oxidized PS, both products namely the free fatty acid and lyso-PS product release were quantified. For PS and oxidized PS, quantifying both products yielded similar rates of product release.

Mouse studies

All mouse studies described in this paper received formal approval from the Indian Institute of Science Education and Research, Pune – Institutional Animal Ethics Committee (IISER-P IAEC) following the guidelines outlined by the Committee for the Purpose of Control and Supervision of Experiments on Animals (CPCSEA), Government of India. Primary peritoneal macrophages were elicited by intraperitoneal injections of 4% (w/v) thioglycollate (3 mL), and harvested using standard protocols56. Cell culturing, compound treatments and LPS stimulation were done as per previously established protocols57. All intraperitoneal LPS injections for systemic (neuro)inflammation were performed using an established protocol for high dose acute (20 mg/kg, 6 h), and low dose chronic (1 mg/kg, q.d., 4 d) treatment paradigm41,58.

Synthesis and characterization of MGR1 and MGR2

See Supplementary Note for complete information on the synthesis and chemical characterization of MGR1 and MGR2.

Superoxide detection from MGR121,22

A luminol stock solution (4 mM) was prepared by dissolving 7.1 mg luminol in 10 mL of 30 mM sodium hydroxide solution and stored on ice. A 2.5 mM stock solution of compounds MGR1 and MGR2 were prepared in DMSO. In the control experiment, 2 μL of MGR1 or MGR2 (25 μM), 5 μL of luminol was added to 193 μL of phosphate buffer pH 8.0 (50 mM). In another set serving as esterase activated set 2.0 μL of MGR1 or MGR2 (25 μM), 5 μL of luminol and 2 μL of esterase (1U/ mL) was added to 191 μL of phosphate buffer pH 8.0 (50 mM). The resulting mixture was incubated at 37 °C and chemiluminescence from reaction mixture was measured using a microwell plate reader (Thermofisher Scientific Varioskan Flash). The HPLC based superoxide detection using hydroethidine was performed using a previously detailed protocol22.

HPLC decomposition study for MGR1 and MGR2

A 10 mM stock of compounds (MGR1, MGR2, JCHD17 and 1-naphthol) in DMSO and 1U/mL stock of porcine liver esterase (Sigma Aldrich) in DPBS were prepared. In the control experiment, 5 μL of respective compound stock (MGR1 or MGR2 or JCHD or 1-naphthol, 100 μM final concentration) was added to 495 μL of DPBS at 37 ºC. In another set, serving as esterase activated set 5 μL of MGR1 or MGR2 (100 μM), 250 μL of esterase (0.5 U/ mL) was added to 245 μL of DBPS at 37 ºC. After 30 min, the reaction mixture was filtered (0.22 μm) and injected (50 μL) in HPLC system (Agilent) with a diode-array

detector (detection wavelength was 315 nm for MGR1 and 280 nm for MGR2) and C18 column (4.6X250 mm, 5 μm). A mobile phase of water: ACN was used with a run time of 25 min using multistep gradient with a flow rate of 1 mL/min – starting with 70:30% → 0 min, 50:50% → 0-5 min, 40:60% → 5-7 min, 30:70% → 7-10 min, 20:80% → 10-15 min, 40:60% → 15-18 min, 60:40% → 18-20 min, 70:30% → 20-25 min (H_2O: ACN).

Statistical analysis

All statistical analyses were performed using the Prism 7 for Mac OS X (GraphPad) software. All data are shown as mean ± s. e. m. unless mentioned otherwise. The Student's two-tailed *t-test* was used to ascertain statistically significant differences between the different study group, where a p-value < 0.05 was considered statistically significant for this study.

Supplementary Material

Refer to Web version on PubMed Central for supplementary material.

Acknowledgements

This work was supported by grants from the Wellcome Trust DBT India Alliance (IA/I/15/2/502058 to S.S.K.), DST-SERB (ECR/2016/001261 to S.S.K; EMR/2015/000668 to H.C.), DBT (BT/PR15848/MED/29/1025/2016 to H. C.), and DST-FIST (Infrastructure Development to IISER Pune Biology Department). Benjamin F. Cravatt, The Scripps Research Institute, is thanked for providing chemical compounds, inhibitors and ABHD12 knockout mice used in this study, and for insightful comments on the manuscript. Nagaraj Balasubramanian, IISER Pune, is thanked for access to the EVOS Imaging System for the chemiluminescence experiments. The National Facility for Gene Function in Health and Disease, IISER Pune is thanked for maintaining and providing mice for this study.

References

1. Aruoma OI. Free radicals, oxidative stress, and antioxidants in human health and disease. J Am Oil Chem Soc. 1998; 75:199–212. DOI: 10.1007/s11746-998-0032-9
2. Niedzielska E, et al. Oxidative Stress in Neurodegenerative Diseases. Molecular neurobiology. 2015; doi: 10.1007/s12035-015-9337-5
3. Finkel T, Holbrook NJ. Oxidants, oxidative stress and the biology of ageing. Nature. 2000; 408:239–247. DOI: 10.1038/35041687 [PubMed: 11089981]
4. Liou GY, Storz P. Reactive oxygen species in cancer. Free Radic Res. 2010; 44:479–496. DOI: 10.3109/10715761003667554 [PubMed: 20370557]
5. Imlay JA. The molecular mechanisms and physiological consequences of oxidative stress: lessons from a model bacterium. Nat Rev Microbiol. 2013; 11:443–454. DOI: 10.1038/nrmicro3032 [PubMed: 23712352]
6. Porter NA. A perspective on free radical autoxidation: the physical organic chemistry of polyunsaturated fatty acid and sterol peroxidation. J Org Chem. 2013; 78:3511–3524. DOI: 10.1021/jo4001433 [PubMed: 23445181]
7. Yin H, Xu L, Porter NA. Free radical lipid peroxidation: mechanisms and analysis. Chem Rev. 2011; 111:5944–5972. DOI: 10.1021/cr200084z [PubMed: 21861450]
8. Spickett CM, Pitt AR. Oxidative lipidomics coming of age: advances in analysis of oxidized phospholipids in physiology and pathology. Antioxid Redox Signal. 2015; 22:1646–1666. DOI: 10.1089/ars.2014.6098 [PubMed: 25694038]
9. Smith WL, Murphy RC. Oxidized lipids formed non-enzymatically by reactive oxygen species. J Biol Chem. 2008; 283:15545–15549. [PubMed: 18285329]

10. Vance JE, Tasseva G. Formation and function of phosphatidylserine and phosphatidylethanolamine in mammalian cells. Biochim Biophys Acta. 2013; 1831:543–554. DOI: 10.1016/j.bbalip.2012.08.016 [PubMed: 22960354]
11. Leventis PA, Grinstein S. The distribution and function of phosphatidylserine in cellular membranes. Annual review of biophysics. 2010; 39:407–427.
12. Hazen SL. Oxidized phospholipids as endogenous pattern recognition ligands in innate immunity. J Biol Chem. 2008; 283:15527–15531. [PubMed: 18285328]
13. Greenberg ME, et al. Oxidized phosphatidylserine-CD36 interactions play an essential role in macrophage-dependent phagocytosis of apoptotic cells. J Exp Med. 2006; 203:2613–2625. DOI: 10.1084/jem.20060370 [PubMed: 17101731]
14. Kagan VE, et al. A role for oxidative stress in apoptosis: oxidation and externalization of phosphatidylserine is required for macrophage clearance of cells undergoing Fas-mediated apoptosis. J Immunol. 2002; 169:487–499. [PubMed: 12077280]
15. Fiskerstrand T, et al. Mutations in ABHD12 cause the neurodegenerative disease PHARC: An inborn error of endocannabinoid metabolism. Am J Hum Genet. 2010; 87:410–417. [PubMed: 20797687]
16. Chen DH, et al. Two novel mutations in ABHD12: expansion of the mutation spectrum in PHARC and assessment of their functional effects. Hum Mutat. 2013; 34:1672–1678. [PubMed: 24027063]
17. Dharmaraja AT, Chakrapani H. A small molecule for controlled generation of reactive oxygen species (ROS). Org Lett. 2014; 16:398–401. DOI: 10.1021/ol403300a [PubMed: 24372330]
18. Dharmaraja AT, Alvala M, Sriram D, Yogeeswari P, Chakrapani H. Design, synthesis and evaluation of small molecule reactive oxygen species generators as selective Mycobacterium tuberculosis inhibitors. Chemical communications. 2012; 48:10325–10327. DOI: 10.1039/c2cc35343a [PubMed: 22977884]
19. Tyagi P, Dharmaraja AT, Bhaskar A, Chakrapani H, Singh A. Mycobacterium tuberculosis has diminished capacity to counteract redox stress induced by elevated levels of endogenous superoxide. Free Radic Biol Med. 2015; 84:344–354. DOI: 10.1016/j.freeradbiomed.2015.03.008 [PubMed: 25819161]
20. Long JZ, Cravatt BF. The metabolic serine hydrolases and their functions in mammalian physiology and disease. Chem Rev. 2011; 111:6022–6063. [PubMed: 21696217]
21. Huu TP, Marquetty C, Pasquier C, Hakim J. Luminol assay for microdetermination of superoxide dismutase activity: its application to human fetal blood. Anal Biochem. 1984; 142:467–472. [PubMed: 6549371]
22. Zhao H, et al. Detection and characterization of the product of hydroethidine and intracellular superoxide by HPLC and limitations of fluorescence. Proc Natl Acad Sci U S A. 2005; 102:5727–5732. DOI: 10.1073/pnas.0501719102 [PubMed: 15824309]
23. McCormack D, McFadden D. A review of pterostilbene antioxidant activity and disease modification. Oxid Med Cell Longev. 2013; 2013doi: 10.1155/2013/575482
24. Kerksick C, Willoughby D. The antioxidant role of glutathione and N-acetyl-cysteine supplements and exercise-induced oxidative stress. J Int Soc Sports Nutr. 2005; 2:38–44. DOI: 10.1186/1550-2783-2-2-38 [PubMed: 18500954]
25. Liebeke M, et al. Depletion of thiol-containing proteins in response to quinones in Bacillus subtilis. Mol Microbiol. 2008; 69:1513–1529. DOI: 10.1111/j.1365-2958.2008.06382.x [PubMed: 18673455]
26. O'Brien PJ. Molecular mechanisms of quinone cytotoxicity. Chem Biol Interact. 1991; 80:1–41. [PubMed: 1913977]
27. Weerapana E, et al. Quantitative reactivity profiling predicts functional cysteines in proteomes. Nature. 2010; 468:790–795. DOI: 10.1038/nature09472 [PubMed: 21085121]
28. Speers AE, Adam GC, Cravatt BF. Activity-based protein profiling in vivo using a copper(i)-catalyzed azide-alkyne [3 + 2] cycloaddition. J Am Chem Soc. 2003; 125:4686–4687. DOI: 10.1021/ja034490h [PubMed: 12696868]
29. Zschornig K, Schiller J. A simple method to generate oxidized phosphatidylcholines in amounts close to one milligram. Chem Phys Lipids. 2014; 184:30–37. DOI: 10.1016/j.chemphyslip.2014.09.003 [PubMed: 25240238]

30. Pathak D, Mehendale N, Singh S, Mallik R, Kamat SS. Lipidomics Suggests a New Role for Ceramide Synthase in Phagocytosis. ACS Chem Biol. 2018; 13:2280–2287. DOI: 10.1021/acschembio.8b00438 [PubMed: 29963848]
31. Knittelfelder OL, Kohlwein SD. Thin-Layer Chromatography to Separate Phospholipids and Neutral Lipids from Yeast. Cold Spring Harb Protoc. 2017; 2017doi: 10.1101/pdb.prot085456
32. Kamat SS, et al. Immunomodulatory lysophosphatidylserines are regulated by ABHD16A and ABHD12 interplay. Nat Chem Biol. 2015; 11:164–171. DOI: 10.1038/nchembio.1721 [PubMed: 25580854]
33. Nomura DK, Casida JE. Lipases and their inhibitors in health and disease. Chem Biol Interact. 2016; 259:211–222. DOI: 10.1016/j.cbi.2016.04.004 [PubMed: 27067293]
34. Wu C, Jin X, Tsueng G, Afrasiabi C, Su AI. BioGPS: building your own mash-up of gene annotations and expression profiles. Nucleic Acids Res. 2016; 44:D313–316. DOI: 10.1093/nar/gkv1104 [PubMed: 26578587]
35. Hoover HS, Blankman JL, Niessen S, Cravatt BF. Selectivity of inhibitors of endocannabinoid biosynthesis evaluated by activity-based protein profiling. Bioorg Med Chem Lett. 2008; 18:5838–5841. DOI: 10.1016/j.bmcl.2008.06.091 [PubMed: 18657971]
36. Liu Y, Patricelli MP, Cravatt BF. Activity-based protein profiling: the serine hydrolases. Proc Natl Acad Sci U S A. 1999; 96:14694–14699. [PubMed: 10611275]
37. Long JZ, et al. Metabolomics annotates ABHD3 as a physiologic regulator of medium-chain phospholipids. Nat Chem Biol. 2011; 7:763–765. [PubMed: 21926997]
38. Ramanadham S, et al. Calcium-independent phospholipases A2 and their roles in biological processes and diseases. J Lipid Res. 2015; 56:1643–1668. DOI: 10.1194/jlr.R058701 [PubMed: 26023050]
39. Blankman JL, Long JZ, Trauger SA, Siuzdak G, Cravatt BF. ABHD12 controls brain lysophosphatidylserine pathways that are deregulated in a murine model of the neurodegenrative disease PHARC. Proc Natl Acad Sci USA. 2013; 110:1500–1505. [PubMed: 23297193]
40. Hsu HY, Wen MH. Lipopolysaccharide-mediated reactive oxygen species and signal transduction in the regulation of interleukin-1 gene expression. J Biol Chem. 2002; 277:22131–22139. DOI: 10.1074/jbc.M111883200 [PubMed: 11940570]
41. Viader A, et al. A chemical proteomic atlas of brain serine hydrolases identifies cell type-specific pathways regulating neuroinflammation. Elife. 2016; 5doi: 10.7554/eLife.12345
42. You LH, et al. Astrocyte Hepcidin Is a Key Factor in Lps-Induced Neuronal Apoptosis. Am J Hematol. 2017; 92:E240–E240.
43. Hou C, et al. Development of a Positron Emission Tomography Radiotracer for Imaging Elevated Levels of Superoxide in Neuroinflammation. ACS Chem Neurosci. 2018; 9:578–586. DOI: 10.1021/acschemneuro.7b00385 [PubMed: 29099578]
44. Matsura T, et al. The presence of oxidized phosphatidylserine on Fas-mediated apoptotic cell surface. Biochim Biophys Acta. 2005; 1736:181–188. DOI: 10.1016/j.bbalip.2005.08.011 [PubMed: 16168707]
45. Joshi A, et al. Biochemical characterization of the PHARC associated serine hydrolase ABHD12 reveals its preference for very long chain lipids. J Biol Chem. 2018; doi: 10.1074/jbc.RA118.005640
46. Blankman JL, Simon GS, Cravatt BF. A Comprehensive Profile of Brain Enzymes that Hydrolyze the Endocannabinoid 2-Arachidonoylglycerol. Chem Biol. 2007; 14:1347–1356. [PubMed: 18096503]
47. Niphakis MJ, et al. A Global Map of Lipid-Binding Proteins and Their Ligandability in Cells. Cell. 2015; 161:1668–1680. DOI: 10.1016/j.cell.2015.05.045 [PubMed: 26091042]
48. Hulce JJ, Cognetta AB, Niphakis MJ, Tully SE, Cravatt BF. Proteome-wide mapping of cholesterol-interacting proteins in mammalian cells. Nat Methods. 2013; 10:259–264. DOI: 10.1038/nmeth.2368 [PubMed: 23396283]
49. Rosenson RS, Stafforini DM. Modulation of oxidative stress, inflammation, and atherosclerosis by lipoprotein-associated phospholipase A2. J Lipid Res. 2012; 53:1767–1782. DOI: 10.1194/jlr.R024190 [PubMed: 22665167]

50. Shimanaka Y, et al. Omega-3 fatty acid epoxides are autocrine mediators that control the magnitude of IgE-mediated mast cell activation. Nat Med. 2017; 23:1287–1297. DOI: 10.1038/nm.4417 [PubMed: 29035365]
51. Folch J, Lees M, Sloane Stanley GH. A simple method for the isolation and purification of total lipides from animal tissues. J Biol Chem. 1957; 226:497–509. [PubMed: 13428781]
52. Simon GM, Cravatt BF. Activity-based proteomics of enzyme superfamilies: serine hydrolases as a case study. J Biol Chem. 2010; 285:11051–11055. [PubMed: 20147750]
53. Inloes JM, et al. The hereditary spastic paraplegia-related enzyme DDHD2 is a principal brain triglyceride lipase. Proc Natl Acad Sci U S A. 2014; 111:14924–14929. DOI: 10.1073/pnas.1413706111 [PubMed: 25267624]
54. Rappsilber J, Mann M, Ishihama Y. Protocol for micro-purification, enrichment, pre-fractionation and storage of peptides for proteomics using StageTips. Nature protocols. 2007; 2:1896–1906. DOI: 10.1038/nprot.2007.261 [PubMed: 17703201]
55. Cox J, Mann M. MaxQuant enables high peptide identification rates, individualized p.p.b.-range mass accuracies and proteome-wide protein quantification. Nat Biotechnol. 2008; 26:1367–1372. DOI: 10.1038/nbt.1511 [PubMed: 19029910]
56. Fahy E, Sud M, Cotter D, Subramaniam S. LIPID MAPS online tools for lipid research. Nucleic Acids Res. 2007; 35:W606–612. DOI: 10.1093/nar/gkm324 [PubMed: 17584797]
57. Hsu KL, et al. DAGLbeta inhibition perturbs a lipid network involved in macrophage inflammatory responses. Nat Chem Biol. 2012; 8:999–1007. [PubMed: 23103940]
58. Nomura DK, et al. Endocannabinoid hydrolysis generates brain prostaglandins that promote neuroinflammation. Science. 2011; 334:809–813. DOI: 10.1126/science.1209200 [PubMed: 22021672]

Europe PMC Funders Author Manuscripts

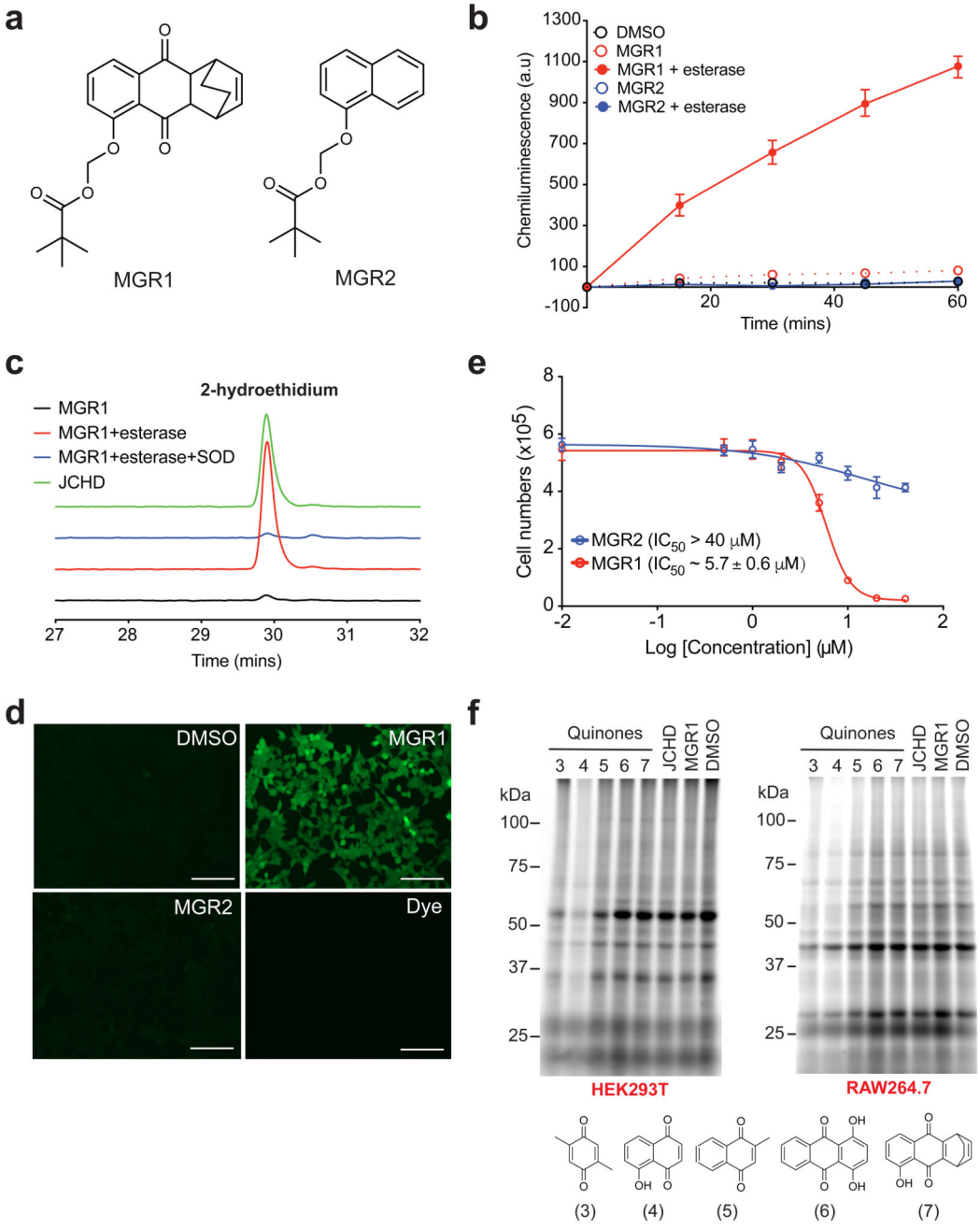

Figure 1. Characterization of a ROS generating probe (MGR1), and an inactive control probe (MGR2).

(**a**) Chemical structures of the active dihydroquinone ROS generator, MGR1 (**1**), and the inactive 1-naphthol control compound, MGR2 (**2**). (**b**) Luminol based chemiluminescence assay showing robust *in vitro* superoxide production by MGR1, but not MGR2, in the presence of esterase. The assay was performed at 37 °C, and each time point represents mean ± SEM of chemiluminescence intensity from three independent experiments. (**c**) HPLC traces, showing the robust formation of superoxide (2-hydroxyethidium formation

Europe PMC Funders Author Manuscripts

from hydroethidine) from MGR1 in the presence of esterase. This superoxide production from MGR1 in the presence of an esterase was ablated by SOD. JCHD was used as a positive control in this experiment. This experiment was performed in triplicate with reproducible results. (**d**) Chemifluorescence showing the robust cellular production of ROS by MGR1, but not MGR2, in HEK293T cells treated with MGR1 or MGR2 (25 μM, 1 h), and subsequently chased with 10 μM DCF, 10 min. The white bar on each image represents 200-μm. The assay was performed as per manufacturers instructions as three independent experiments with reproducible results. Also see Supplementary Fig. 5 for more information. (**e**) Cell viability assay showing cell death of HEK293T cells by higher concentration of MGR1 (> 5 μM), but not MGR2, due to heightened ROS production. Data represents mean ± SEM for 4 independent replicates, and the 95% interval for the reported half maximal inhibition constant (IC_{50}) value of MGR1 is 5.1 – 6.3 μM. (**f**) Gel based chemoproteomics showing negligible proteome wide thiol reactivity of MGR1 treated with esterase compared to other reactive quinones (3 – 7) in HEK293T and RAW264.7 cell lysates. All compounds were used at 100 μM for 1 h, and subsequently chased with 1 mM IAA (1 h), following which click reaction was performed. This experiment was performed in triplicates with reproducible results.

Europe PMC Funders Author Manuscripts

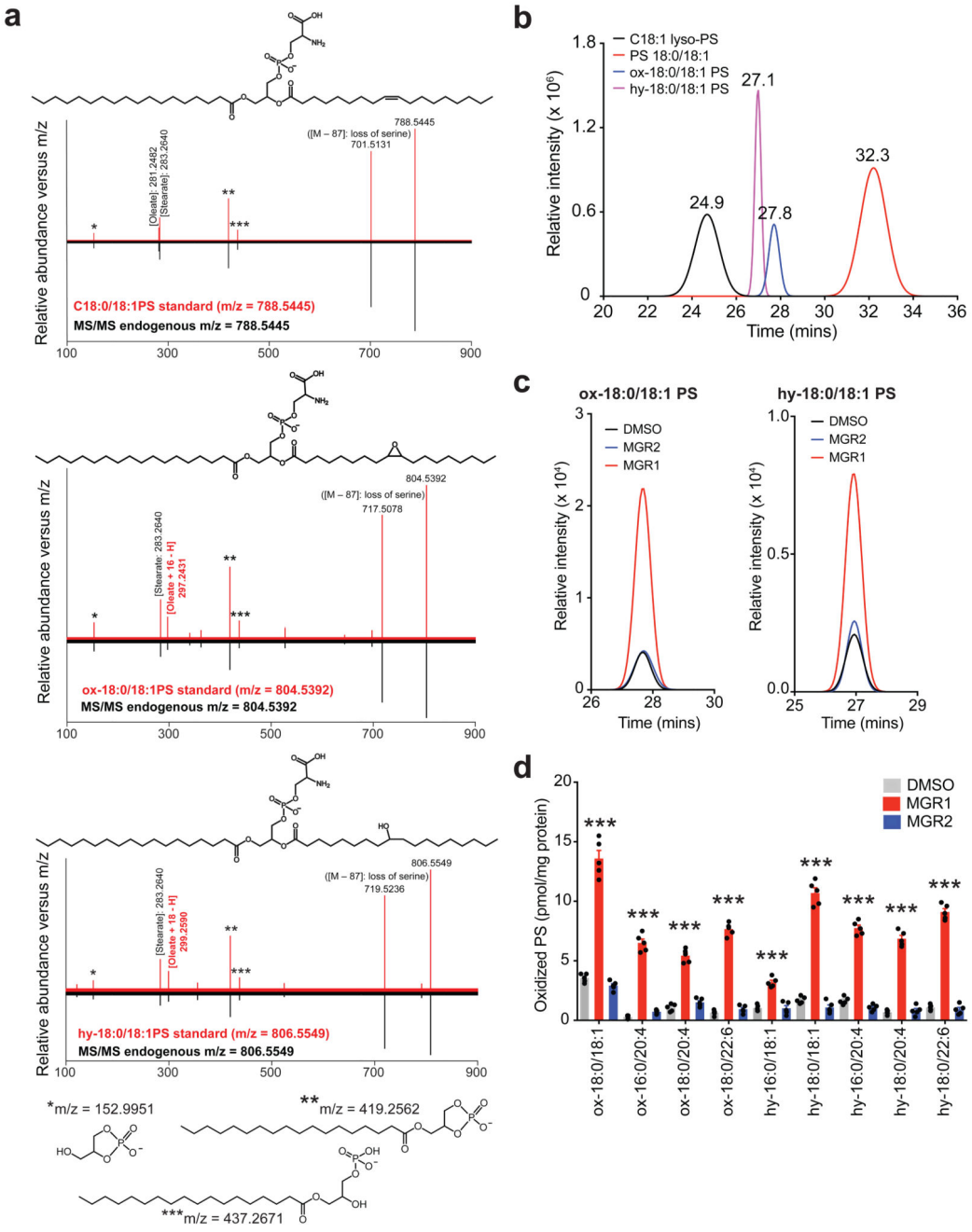

Figure 2. Characterization and quantification of oxidized PS in mammalian cells following MGR1 treatment.

(**a**) MS/MS fragmentation for the lipids standards (red trace) for C18:0/18:1PS, ox-18:0/18:1PS and hy-18:0/18:1PS, and the corresponding endogenous phospholipids (black trace) of m/z 788.5445, 804.5392 and 806.5549 from HEK293T cells treated with MGR1 (2 μM, 4 h). The daughter ions common to all masses from the MS/MS analysis include 152.9951 (dehydo-glycerophosphate), 283.2640 (stearate), 419.2562 (dehydro-1-stearoyl-lysophosphatidic acid), and 437.2671 (1-stearoyl-lysophosphatidic acid), and

[parent m/z – 87.0315] peak (loss of serine). The key daughter ions distinguishing the three species (denoted in red text) are 281.2481 (oleate for m/z = 788.5445), 297.2431 (oleate + 16 amu for m/z = 804.5392), and 299.2590 (oleate + 18 amu for m/z = 806.5549). This MS/MS fragmentation study was performed in triplicate with reproducible results. (**b**) The LC-MS elution profile for the lipids standards for C18:1 lyso-PS, C18:0/18:1PS, ox-18:0/18:1PS and hy-18:0/18:1PS, showing the increased hydrophilicity of ox-18:0/18:1PS and hy-18:0/18:1PS, compared to C18:0/18:1PS. The LC elution profiles were performed in duplicates with reproducible results. (**c**) LC-MS/MS traces (MRM-HR) for ox-18:0/18:1PS (m/z = 804.5) and hy-18:0/18:1PS (m/z = 806.6) extracted from HEK293T cells treated with MGR1 (2 μM) or MGR2 (2 μM) or DMSO (all 4 h), showing robust increases for ox-18:0/18:1PS and hy-18:0/18:1PS, following MGR1, but not MGR2 or DMSO treatment. This experiment was done in triplicates with reproducible results. (**d**) Targeted LC-MS/MS MRM-HR measurements of oxidized PS from HEK293T cells treated 4 h with MGR1 (2 μM) or MGR2 (2 μM) or DMSO. Data represents mean ± SEM for 5 independent replicates per group. Student's t-test (two-tailed): *** $p < 0.001$ versus DMSO group. See Supplementary Dataset 2 for complete list of quantified lipids and detailed p-values.

Europe PMC Funders Author Manuscripts

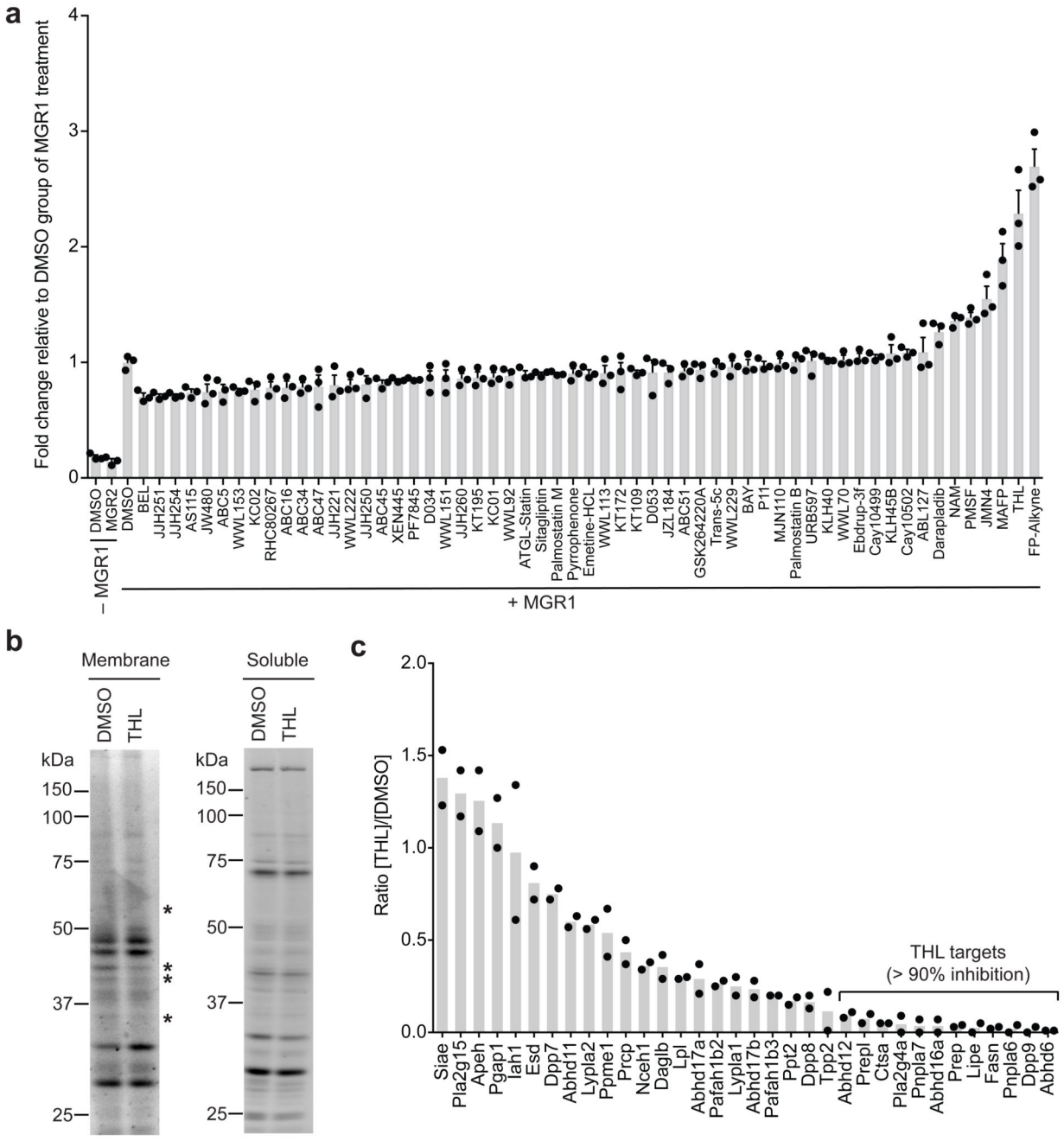

Figure 3. Chemical genetic screen to identify oxidized PS lipase(s) in mammalian cells.

(**a**) Relative oxidized PS levels from RAW264.7 cells from a highly focused chemical genetic screen of 57 known lipase inhibitors. Data is represented relative levels compared DMSO group of MGR1 treated control. Each group represents mean ± SEM for 3 biological replicates. A two-fold increase in oxidized PS was set as a threshold to identify hits in this screen. (**b**) ABPP gel of the membrane and soluble proteomes of RAW264.7 cells treated with THL (10 μM, 4 h) or DMSO using FP-rhodamine (2 μM, 37 °C, 45 min). The asterisks (*) represent SH activities inhibited by THL in the membrane proteome. The ABPP gels

Europe PMC Funders Author Manuscripts

were done in triplicate with reproducible results. (**c**) ABPP-ReDiMe LC-MS/MS analysis for SH activities from RAW264.7 cells treated *in situ* with THL (10 μM, 4 h). Data represents mean for two independent proteomics experiments, where each replicate corresponds to the median heavy/light ratio (THL = light, DMSO= heavy) for total quantified peptide for each serine hydrolase enzyme. A cut off of ≥ 2 quantified peptides per SH was required for this analysis. See Supplementary Dataset 4 for complete ABPP-ReDiMe datasets.

Europe PMC Funders Author Manuscripts

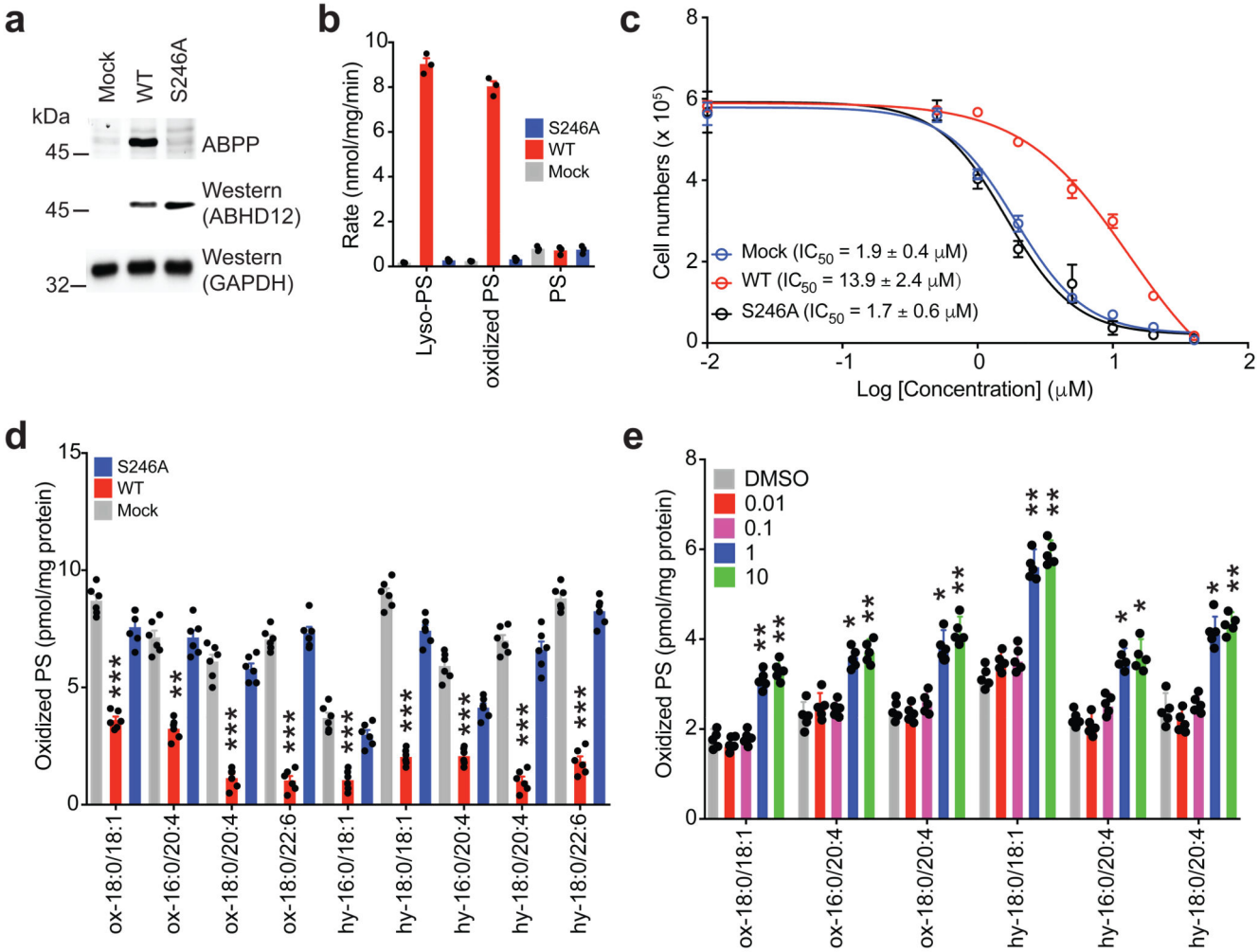

Figure 4. Biological validation of human ABHD12 as an oxidized PS lipase.

(**a**) ABPP gel and western blot on the membrane proteomes of HEK293T cells transiently transfected with mock, or wild type (WT) human ABHD12 (hABHD12), or active site S246A hABHD12 mutant. ABPP gel (2 μM FP-rhodamine, 45 min, 37 °C) shows robust activity for WT, but not S246A hABHD12 or mock proteomes, while the western blot (anti-ABHD12, rabbit, Abcam, 182011) confirms overexpression of WT and S246A hABHD12 over mock. The ABPP gel and western blot analysis were performed in triplicates with reproducible results each time. GAPDH was used as a loading control for these experiments. Full gel images are available in Supplementary Fig. 26. (**b**) Substrate assays of membrane proteomes from HEK293T cells transfected with mock, WT or S246A hABHD12, showing robust hydrolysis of lyso-PS (C18:1) and oxidized PS (ox-C18:0/18:1PS + hy-18:0/18:1PS) by WT, but not S246A hABHD12 or mock proteomes. All proteomes showed negligible activity for the C18:0/18:1PS. The data represents mean ± SEM for 3 independent experiments. (**c**) Cell viability assay on HEK293T cells transfected with mock, or WT or S246A hABHD12 treated with increasing concentrations of MGR1 (0 – 40 μM, 4 h), showing increased cellular viability for WT hABHD12 transfected HEK293T cells following MGR1 treatment compared to mock or S246A hABHD12 transfected HEK293T

cells. Data represents mean ± SEM for 4 biological replicates, and the 95% interval for the reported IC_{50} values of MGR1 for mock, WT and S246A is 1.5 – 2.3, 11.5 – 16.3 and 1.3 – 2.3 μM respectively. (**d**) Cellular oxidized PS for HEK293T cells transfected with mock, or WT or S246A hABHD12, and treated with MGR1 (2 μM, 4 h). The WT hABHD12 transfected HEK293T cells have substantially lower oxidized PS compared to other groups. Data represents mean ± SEM for 6 biological replicates per group. Student's t-test (two-tailed): ** $p < 0.01$, *** $p < 0.001$ versus mock group. See Supplementary Dataset 2 for complete list of quantified lipids and detailed p-values. (**e**) Pharmacological blockade of ABHD12 in RAW264.7 cells with increasing THL dosing (0 – 10 μM, 4 h) causes accumulation in cellular oxidized PS. Data represents mean ± SEM for 5 biological replicates per group. Student's t-test (two-tailed): * $p < 0.05$, ** $p < 0.01$ versus DMSO group.

Europe PMC Funders Author Manuscripts

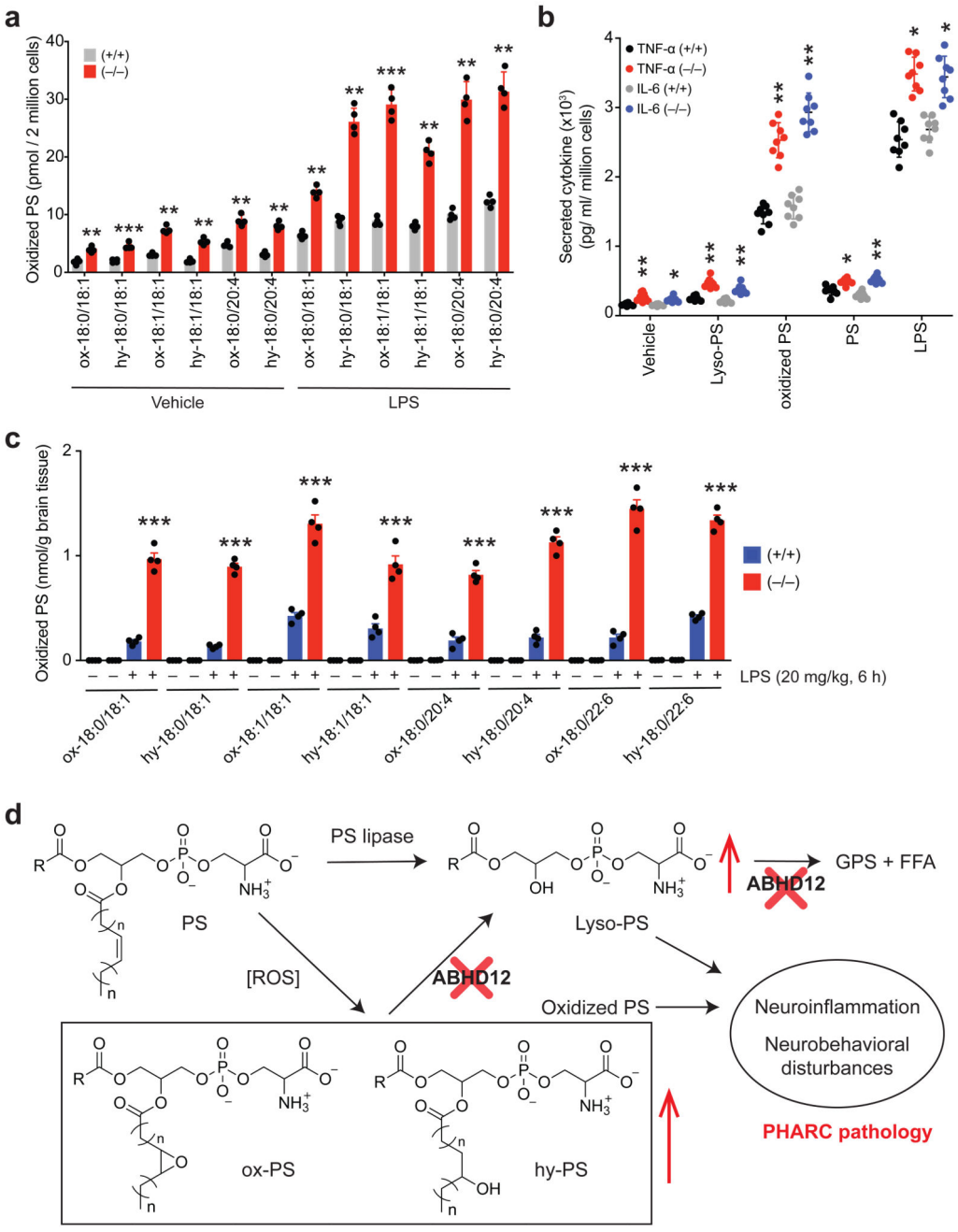

Figure 5. ABHD12 functions as an oxidized PS lipase *in vivo*.

(**a**) Cellular oxidized PS levels in mouse primary peritoneal macrophages (PPM) harvested from wild type (+/+) or ABHD12 knockout (–/–) mice, following vehicle (sterile DPBS) or LPS stimulation (10 μg/mL) for 4 h. Data represents mean ± SEM for 4 independent experiments per group. Student's t-test (two-tailed): ** $p < 0.01$, *** $p < 0.001$ for (–/–) versus (+/+) group. See Supplementary Dataset 2 for complete list of quantified lipids and detailed p-values. (**b**) Secreted concentrations of proinflammatory cytokines TNF-α and IL-6 from mouse PPM from WT (+/+) and ABHD12 knockout (–/–) mice treated with

Europe PMC Funders Author Manuscripts

vehicle (sterile DPBS), C18:1 lyso-PS, oxidized PS (ox-18:0/18:1PS + hy-18:0/18:1PS), C18:0/18:1PS, or LPS (10 μg/mL, 4 h). Data represents mean ± SEM for 8 independent experiments per group. Student's t-test (two-tailed): * $p < 0.05$, ** $p < 0.01$ for (–/–) versus (+/+) group. (**c**) Oxidized PS concentrations in the brains of wild type (+/+) or ABHD12 knockout (–/–) mice undergoing high dose acute LPS treatment (20 mg/kg, 6 h, intraperitoneal injections). The data suggests the increased accumulation of oxidized PS for (–/–) compared to the (+/+) group in this treatment regime. Data represents mean ± SEM for 4 independent experiments per group. Student's t-test (two-tailed): ** $p < 0.01$, *** $p < 0.001$ for (–/–) versus (+/+) group. See Supplementary Dataset 2 for complete list of quantified lipids and detailed p-values. (**d**) A model implicating oxidized PS lipids in the pathology of the neurological disorder, PHARC. Previous studies in a murine model for PHARC have shown that ABHD12 regulates levels of lyso-PS in mammalian brain and immune system32,39, and hence lyso-PS has been attributed to the neuroinflammation and neurobehavioral disturbances seen in human PHARC patients39. Here, we show that ABHD12 also controls the levels of oxidized PS in different mammalian systems including primary mouse macrophages and the brain under oxidative stress. Based on previous immunological studies, which suggest a role for oxidized PS in cellular apoptosis, we add onto the existing model describing the pathology of PHARC; where oxidized PS produced from surplus ROS during oxidative stress may along with lyso-PS, contribute synergistically towards the pathology of this neurological disorder.